

EFFECT OF IRRADIATION SPECTRUM ON THE MICROSTRUCTURAL EVOLUTION IN CERAMIC INSULATORS - S.J. Zinkle (Oak Ridge National Laboratory)

OBJECTIVE

The objective of this study is to determine examine the effect of variations in the ionizing and displacive radiation environments on the microstructure of oxide ceramic insulators.

SUMMARY

Cross section transmission electron microscopy has been used to investigate the microstructure of $MgAl_2O_4$ (spinel) and Al_2O_3 (alumina) following irradiation with ions of varying mass and energy at room temperature and $650^\circ C$. Dislocation loop formation was suppressed in specimens irradiated with light ions, particularly in the case of spinel. An evaluation of the data showed that dislocation loop formation during irradiation at $650^\circ C$ was suppressed when the ratio of the electronic- to nuclear-stopping power was greater than ~ 10 and ~ 1000 for spinel and alumina, respectively. The effect of uniform background levels of ionizing radiation on the microstructural evolution in spinel was investigated by performing simultaneous dual-beam (He^+ and heavy ion) irradiations. The uniform ionizing radiation source did not affect the microstructural evolution of spinel unless the ionization was very intense (average electronic- to nuclear-stopping power ratio >100). These results clearly indicate that light ion and electron irradiations produce microstructures which are not representative of the microstructure that would form in these ceramics during fission or fusion neutron irradiation.

PROGRESS AND STATUS

1. Introduction

Ceramic insulators such as $MgAl_2O_4$ (spinel) or Al_2O_3 (alumina) are required for several key applications in fusion energy systems that are currently being developed. These applications include magnetic diagnostic coils, insulating feedthroughs and windows for the radiofrequency heating components, and blanket insulators (for systems that utilize liquid metal coolants).¹ The 14 MeV neutrons associated with the DT fusion reaction will produce displacement damage and an intense ionizing radiation field in the materials surrounding the confined plasma. At the present time, there are no available sources for bulk irradiations that match the irradiation spectrum and intensity of proposed DT fusion reactors.

Ion irradiation is a convenient method for studying microstructural changes associated with energetic irradiation. In particular, the effect of irradiation spectrum on the microstructural evolution can be examined by changing the mass and energy of the bombarding ion. Recent ion irradiation studies have shown that the microstructure² and macroscopic properties³⁻⁶ of insulators such as MgO , Al_2O_3 and $MgAl_2O_4$ are sensitive to variations in the ionizing and displacive irradiation spectra. The published studies indicate that irradiation with energetic light ions causes a large reduction in the density of interstitial dislocation loops and produces less volumetric swelling than irradiation with heavy ions at a comparable displacement damage rate and displacement dose. Several possible physical mechanisms have been proposed for this sensitivity to irradiation spectrum, including enhanced point defect recombination due to ionization-enhanced diffusion (IED), and nuclear stopping power effects.^{2,7} The purpose of the present paper is to summarize recent microstructural data obtained on ion-irradiated alumina and spinel which provide further evidence for a strong dependence on irradiation spectrum.

One potential disadvantage associated with ion irradiation is the strong effect of the implanted ions on the microstructural development. As reviewed elsewhere,² the implanted ion region of ceramic insulators contains numerous microstructural features that are generally not found in irradiated regions that are isolated from the implanted ions. In addition, defect cluster formation is generally enhanced in the implanted ion regions. In the present study, ion energies ≥ 1 MeV have been employed to provide sufficient isolation of the implanted ion region from the rest of the irradiated regions.

2. Experimental Procedure

Polycrystalline blocks of Al_2O_3 (GE Lucalox or Wesgo AL995) and MgAl_2O_4 (Ceredyne) were sliced into sheets of 0.5 mm thickness, and 3-mm-diameter transmission electron microscope (TEM) disks were ultrasonically cut from the sheets. The grain size of both the alumina and spinel specimens was about 30 μm . The TEM disks were mechanically polished with 0.5 μm diamond paste, and then bombarded in a 3 x 3 target array at room temperature or 650°C in the triple ion beam accelerator facility at Oak Ridge National Laboratory.⁸ The irradiation temperature was determined from a thermocouple spot-welded to the face of a stainless steel TEM disk (which has a thermal conductivity comparable to the ceramic specimens) that occupied one of the positions in the 9-specimen array. The temperature of the target holder substrate was also continuously measured during the irradiation. The specimen surface temperature (monitored by the thermocouple on the stainless steel TEM disk) was within 20°C of the substrate temperature for all of the irradiations.

The specimen arrays were exposed to ion beams ranging from 1 MeV H^+ to 4 MeV Zr^+ ions. The ion beam fluxes and fluences on different sets of specimen arrays were systematically varied for a given ion beam in order to gain some knowledge about the relative roles of damage rate and cumulative damage level. In addition, several specimen arrays were exposed to simultaneous dual ion beams in order to study the effect of intense uniform ionization on the microstructural evolution. Table 1 summarizes the range of irradiation conditions that were examined. The TRIM-90 computer code⁹ was used to calculate the depth-dependent ionization and displacement damage dose in Al_2O_3 . The TRIM calculations were performed using the measured¹⁰ threshold displacement energies of 24 eV and 78 eV in Al_2O_3 for the aluminum and oxygen sublattices, respectively. The damage level in displacements per atom (dpa) was determined from the damage energy calculated by TRIM, using the modified Kinchin-Pease formula¹¹ and assuming a sublattice-averaged threshold displacement energy of 40 eV. The calculated dpa values for spinel (using an average threshold displacement energy of 40 eV) were similar to those for alumina. The damage rates varied between $\sim 10^{-6}$ and 10^{-3} dpa/s (with corresponding ionizing dose rates of 0.1 to 30 MGy/s), depending on the ion species and flux. As indicated in Table 1, the calculated ratio of electronic- to nuclear-stopping power (ENSP) at a depth of 0.5 μm varied from about 2.4 for the heaviest ion (4 MeV Zr) to about 2000 for the lightest ion (1 MeV H). A portion of the specimen array in some of the irradiations was coated with a thin layer ($\sim 0.1 \mu\text{m}$) of conductive carbon prior to irradiation in order to minimize specimen charging. The microstructure of these carbon-coated specimens following irradiation was found to be identical to that of uncoated specimens in the same target holder, which demonstrated that specimen charging did not have a significant effect on the observed microstructure.

Table 1. Summary of ion irradiation conditions

Ion beam	Fluence levels ($10^{20}/\text{m}^2$)	Flux levels ($10^{16}/\text{m}^2\text{-s}$)	Damage parameters at 0.5 μm depth		
			dpa	MGy/s	ENSP
1 MeV H	3-170	6-60	0.0005-0.03	0.3-3	2000
1 MeV He	1-100	4-40	0.005-0.5	1-10	800
3 MeV C	0.04-4	0.2-2	0.002-0.2	0.1-1	250
2.4 MeV Mg	8-28	11-38	3-10	8-29	20
2 MeV Al	5-40	11	3-23	7	13
3.6 MeV Fe	0.2-1.2	0.5	0.3-2	0.5	6
4 MeV Zr	0.02-2	0.2-0.3	0.08-8	0.2-0.3	2.4
4 MeV Fe & 1 MeV He	0.2-1.2 (Fe) 3.5-21 (He)	0.5 (Fe) 8.5 (He)	0.3-2 (total)	2.5 (total)	28
1.8 MeV Cl & 1 MeV He	0.07-0.4 (Cl) 8-40 (He)	0.17 (Cl) 18 (He)	0.1-0.7 (total)	4.4 (total)	160

Cross-section TEM specimens were prepared by gluing a mechanically polished nonirradiated specimen to the irradiated surface of each sample, sectioning perpendicular to the irradiation surface, mechanically dimpling, and ion milling either at room temperature or in a liquid nitrogen cooled stage (6 keV Ar ions, 15° sputtering angle) until perforation occurred at the glued interface.¹² The specimens were examined in a Philips CM12 electron microscope operating at 120 kV.

3. Results

Figure 1 shows the depth-dependent damage energy in alumina for the different ions used in this study, as calculated with the TRIM⁹ code. The damage energy is directly proportional to the amount of displacement damage created in the ceramic, and is obtained by subtracting the recoil ionization from the nuclear stopping power.¹¹ For each ion, the damage energy reaches a maximum value at a depth comparable to the ion range. The maximum damage energy increases with increasing ion mass, ranging from ~0.70 eV/nm for 1-MeV H⁺ (not shown in Fig. 1) to ~920 eV/nm for 4-MeV Zr⁺ ions. The maximum damage energy is 3 to 25 times the damage energy at the surface, with the largest depth dependence occurring for the lightest ions.

Most of the energy lost by the MeV ion beams is due to interactions with the bound valence electrons in the ceramic. These low-energy interactions produce ionization of the lattice atoms by exciting valence electrons into the conduction band. The electronic stopping power of most ions steadily decreases with increasing depth up to the region where the ions are deposited. In the case of energetic light ions such as 1-MeV H⁺, the electronic stopping power increases slightly with increasing depth up to the implanted ion region. Figure 2 shows the calculated depth-dependent ratio of the electronic- to nuclear-stopping power (ENSP) in alumina for the different ions used in this study. The ENSP ratio is approximately proportional to the amount of ionization per displaced atom (it is not exactly proportional since displacement damage is only due to the damage energy portion of the nuclear stopping power). Energetic light ions such as 1-MeV H⁺ and 1-MeV He⁺ have particularly high ENSP ratios. In all cases, the ENSP ratio is greater than one from the irradiation surface up to depths that are comparable to the ion range.

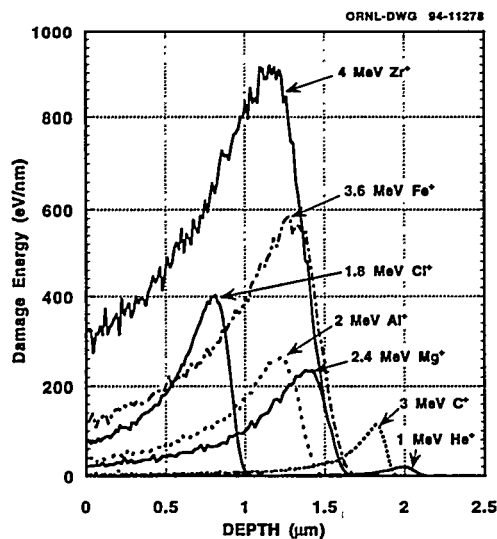


Fig. 1. Calculated depth-dependent damage energy density in Al₂O₃ for various ions.

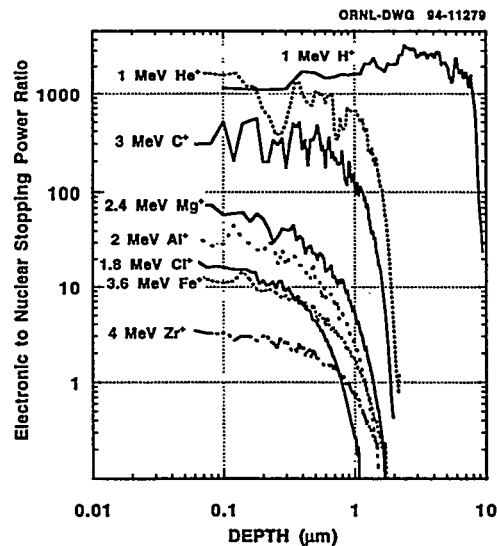


Fig. 2. Calculated ratio of the electronic to nuclear stopping power in Al₂O₃ for various ions.

3.1 Microstructure of irradiated MgAl₂O₄

Figure 3 shows the cross-section microstructure of spinel following irradiation with 4-MeV Zr⁺ ions at 650°C to a fluence of 2×10^{19} Zr⁺/m². The irradiation produced a moderate density (8×10^{20} /m³) of dislocation loops in the midrange region (~ 0.5 μ m depth), and approximately an order of magnitude higher density of loops in the peak damage region that contained the implanted Zr ions. The dislocation loop density was very low ($< 1 \times 10^{19}$ /m³) for regions located within 0.2 μ m of the irradiated surface. The average loop diameter was ~ 15 nm. All of the loops were interstitial in character, with Burgers vectors along $\langle 110 \rangle$ directions. Some of the loops were observed to lie on $\{111\}$ and $\{110\}$ habit planes. However, most of the loop habit planes were intermediate between $\{111\}$ and $\{110\}$ planes. Following the loop sequence outlined by Kinoshita and coworkers,^{7,13} this suggests that most of the loops in this specimen have unfaulted and are in the process of rotating from $\{111\}$ habit planes to $\{110\}$ habit planes.

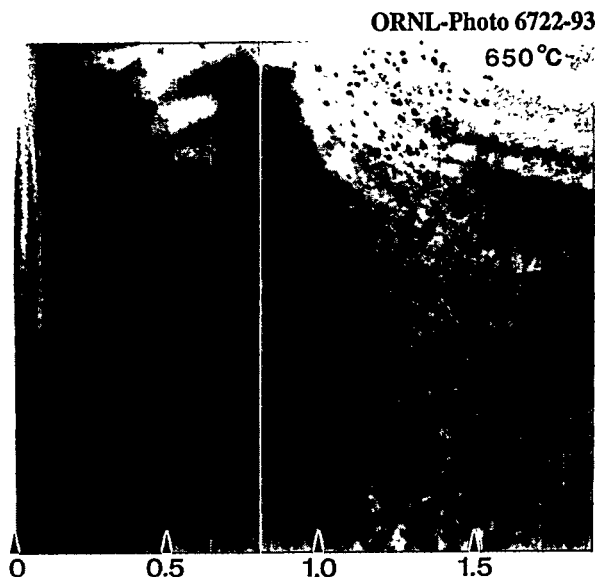


Fig. 3. Depth-dependent microstructure of MgAl₂O₄ irradiated with 4-MeV Zr⁺ ions to a fluence of 2×10^{19} Zr⁺/m².

Examination of spinel specimens irradiated at lower fluences and with different ions allowed the threshold dose for observable defect cluster formation to be determined.¹⁴ The measured threshold dose for observable defect cluster formation was ~ 0.1 dpa, which agrees with other ion¹⁵ and neutron¹⁶ irradiation studies performed on spinel.

The microstructure of spinel irradiated with 4-MeV Zr⁺ ions at room temperature consisted of a high density ($\sim 5 \times 10^{22}$ /m³) of small defect clusters that were rather uniformly distributed throughout the irradiated region. There was no evidence for a defect-free zone near the irradiated surface in specimens irradiated near room temperature, in contrast to the 650°C results. The loop diameter at intermediate depths (~ 0.7 μ m) increased steadily with increasing fluence, with values of ~ 3 nm at 1.5 dpa and ~ 10 nm after a damage level of 10 dpa. Most of the loops were observed to have $\{110\}$ habit planes after high dose irradiation.

The depth-dependent microstructure of spinel irradiated with 3.6-MeV Fe⁺ ions was qualitatively similar to the 4-MeV Zr⁺ results. There was no observable defect cluster formation in regions located within ~ 0.4 μ m of the irradiated surface for specimens irradiated with Fe⁺ ions at 650°C. The Burgers vector was $a/4\langle 110 \rangle$ for most of the dislocation loops analyzed in the specimen irradiated at 650°C to 2 dpa at a depth of 0.5 μ m (1.2×10^{20} Fe⁺/m²). The distribution of loops on the different habit planes varied with irradiation depth. In the midrange region (~ 1 μ m depth), about 75% of the loops were located on $\{110\}$ planes and the remainder were located on $\{111\}$ planes. The fraction of loops with $\{111\}$ habit planes increased to $\sim 70\%$ near the peak damage region. The loop density increased and the loop size decreased with increasing depth from the irradiated surface. The measured loop density and average diameter were 5×10^{20} /m³ and ~ 50 nm at a depth of 0.6 μ m, and 4×10^{21} /m³ and ~ 20 nm at a depth of 1 μ m. Irradiation with Fe⁺ ions at room temperature produced a high density ($\sim 5 \times 10^{22}$ /m³) of small defect clusters with an average diameter near 5 nm. The width of the defect-free zone near the irradiated surface was < 40 nm in the specimens irradiated at room temperature.

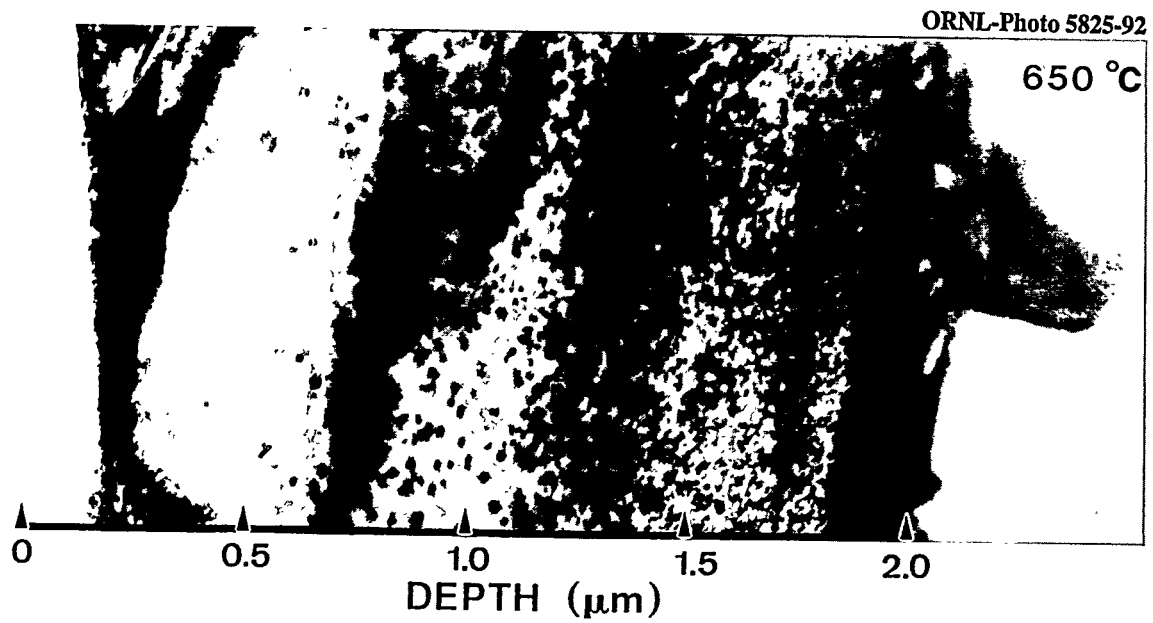


Fig. 4. Depth-dependent microstructure of MgAl₂O₄ irradiated with 2.4-MeV Mg⁺ ions at 650°C to a fluence of 8×10^{20} Mg⁺/m².

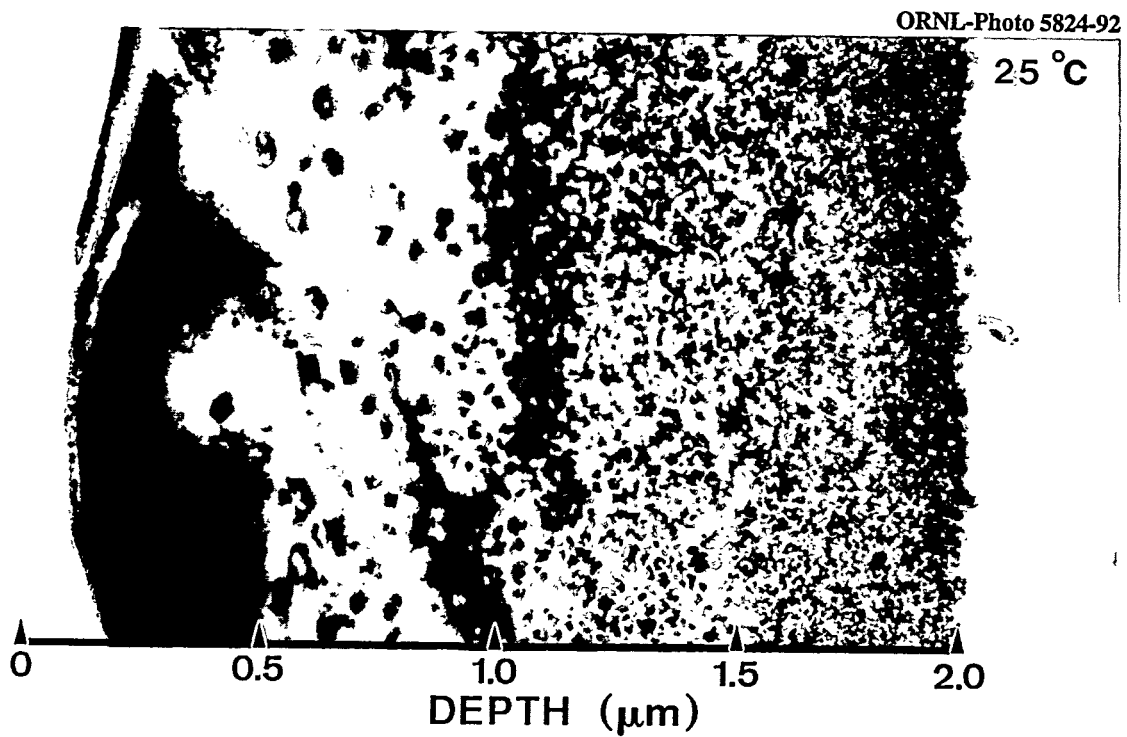


Fig. 5. Depth-dependent microstructure of MgAl₂O₄ irradiated with 2.4-MeV Mg⁺ ions at room temperature to a fluence of 8×10^{20} Mg⁺/m².

The microstructure of spinel irradiated with 2-MeV Al⁺ ions was similar to that observed following Zr⁺ and Fe⁺ ion irradiation. Details of the microstructural analysis have been previously reported.^{17,18} A defect-free zone was observed in regions located within ~0.4 μm of the irradiated surface after irradiation with Al⁺ ions at 650°C. Defect-free zones of comparable width were also observed next to grain boundaries.¹⁷ Irradiation at room temperature reduced the width of this defect-free zone to <50 nm. The fraction of loops with {110} habit planes increased with increasing dose. About 75% of the loops were observed on {110} planes after 3 dpa, and ~90% after 10 dpa. The remaining loops were located on {111} planes. The Burgers vector for almost all of the loops was $a/4\langle 110 \rangle$. A small fraction of the loops on {111} planes had $a/6\langle 111 \rangle$ Burgers vectors.

The depth-dependent microstructure of spinel irradiated with 2.4-MeV Mg⁺ ions at 650°C and room temperature is shown in Figs. 4 and 5, respectively. Microstructural data on spinel specimens irradiated with Mg⁺ ions at slightly higher fluxes have also been reported elsewhere.^{2,14,17,19} In contrast to the heavier ion (Al, Fe and Zr) irradiations, the microstructure in specimens irradiated with Mg⁺ ions at room temperature was similar to that in specimens irradiated at 650°C. The width of the defect-free region adjacent to the irradiated surface varied between 0.5 and 0.9 μm for both irradiation temperatures. The largest denuded zone width occurred in specimens irradiated at the highest particle flux. The loop density in the midrange region increased with increasing depth. It was generally observed that the loop density was higher in the 650°C specimens compared to the room temperature specimens following irradiation to the same total fluence. As discussed later, this effect may be attributable to the ~50% higher particle flux employed for the room temperature Mg⁺ irradiations.

Figure 6 shows the microstructure of spinel following irradiation with 3-MeV C⁺ ions at 650°C to a fluence of 4.6×10^{19} C⁺/m². There was no observable defect cluster formation outside of the implanted ion region (2.1-2.4 μm depth). The damage level at irradiation depths <1.5 μm in this specimen was less than the experimentally-determined threshold level for producing observable defect clusters in spinel (~0.1 dpa) and therefore cannot provide definitive information on possible spectrum effects. On the other hand, the lack of observable dislocation loop formation at depths between 1.5 and 2.1 μm, where the damage level exceeds 0.1 dpa, suggests that C⁺ ions are not effective at producing defect clusters in spinel. A similar large defect-free zone was observed in spinel irradiated with C⁺ ions at room temperature to a fluence of 4×10^{20} C⁺/m² (0.2 dpa at 0.5 μm).

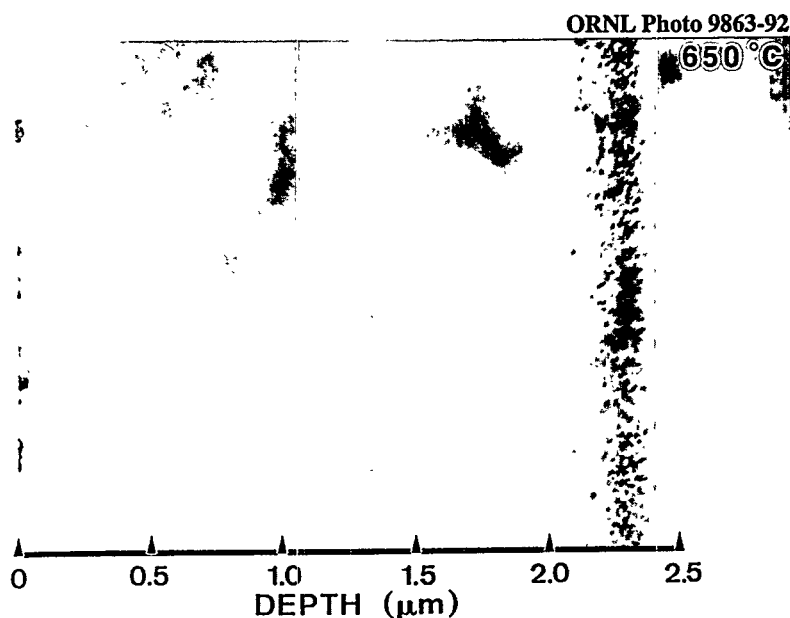


Fig. 6. Depth-dependent microstructure of MgAl₂O₄ irradiated with 3-MeV C⁺ ions to a fluence of 4.6×10^{19} C⁺/m².

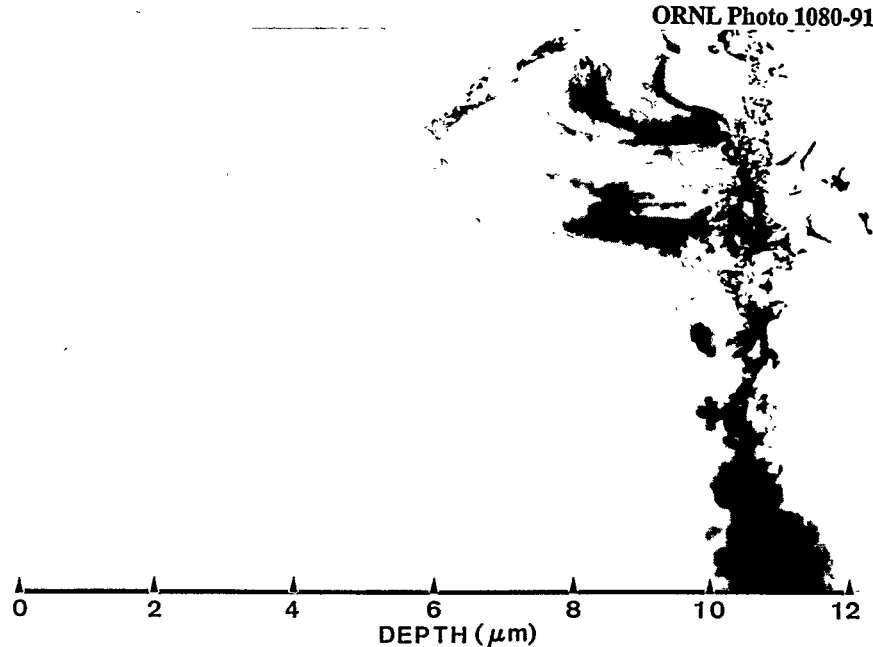


Fig. 7. Depth-dependent microstructure of MgAl_2O_4 irradiated with 1-MeV H^+ ions to a fluence of $1.7 \times 10^{22} \text{ H}^+/\text{m}^2$.

Irradiation of spinel with 1-MeV He^+ or H^+ ions at 650°C did not produce any observable defect cluster formation except in the implanted-ion region. Figure 7 shows an example of the microstructure of spinel following 1-MeV H^+ ion irradiation to a fluence of $1.7 \times 10^{22} \text{ H}^+/\text{m}^2$. The calculated damage level in this specimen was >0.1 dpa over the latter half of the ion range (5-10 μm depths), but there was no evidence of defect cluster formation in this region (except for the implanted ion region). Similarly, high fluence 1-MeV He^+ ion irradiations that produced midrange damage levels of 0.5 to 3 dpa did not result in any observable defect cluster formation.^{2,14,20}

3.2 Microstructure of irradiated Al_2O_3

Alumina was found to be less sensitive than spinel to variations in the irradiation spectrum. Figure 8 shows the microstructure of alumina following irradiation with 2-MeV Al^+ ions at 650°C to a fluence of $9 \times 10^{20} \text{ Al}^+/\text{m}^2$ (5 dpa at 0.5 μm depth). A high density ($\sim 1 \times 10^{23}/\text{m}^3$) of small defect clusters were observed in the irradiated region, without any noticeable depth dependence. An analysis of the dislocation loops indicated that they occurred on both basal (0001) and prism $\{1\bar{1}00\}$ planes, with predominant Burgers vectors of $1/3[0001]$ and $1/3\langle 1\bar{1}00 \rangle$, respectively.¹⁷ The width of the defect-free zones adjacent to the irradiated surface and grain boundaries was <15 nm, which is more than an order of magnitude smaller than that observed in spinel irradiated under comparable conditions.

The microstructure of alumina irradiated with 3-MeV C^+ ions was similar to that observed

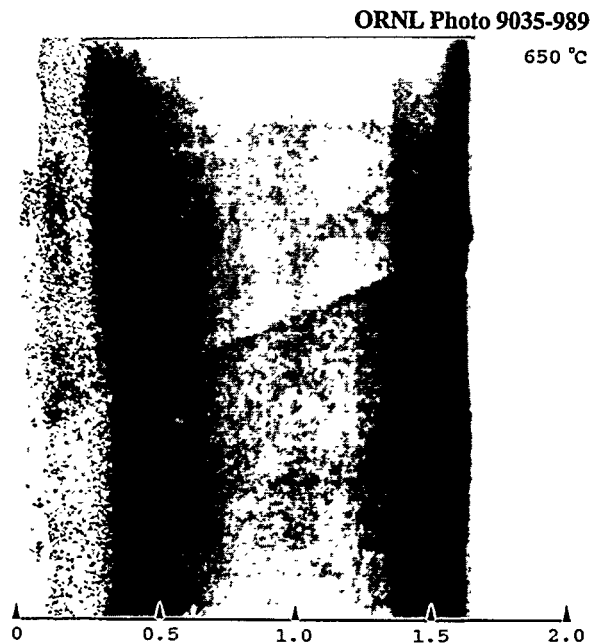


Fig. 8. Depth-dependent microstructure of Al_2O_3 irradiated with 2-MeV Al^+ ions to a fluence of $9 \times 10^{20} \text{ Al}^+/\text{m}^2$.

following irradiation with heavier ions. Figure 9 shows the microstructure after irradiation to a relatively low fluence of $3 \times 10^{19} \text{ C}^+/\text{m}^2$ at 650°C (0.015 dpa at $0.5 \mu\text{m}$ depth). Small dislocation loops were observable throughout the irradiated region in this specimen, indicating that the threshold dose for observable defect cluster formation in alumina at 650°C is ~ 0.01 dpa. The loop size and density increased with increasing depth for this low-fluence irradiation condition. Low-fluence irradiations of alumina performed with different ions produced a similar threshold dose for observable defect cluster formation of ~ 0.01 dpa.¹⁴ This threshold dose is an order of magnitude smaller than the threshold dose obtained for spinel at 650°C (Section 3.1).

Defect clusters were formed throughout the irradiated region in alumina irradiated with 1-MeV He^+ ions at 650°C .^{2,20} However, the loop density was reduced by about a factor of five and the loop size was increased by about a factor of two compared to specimens irradiated with heavier ions to a similar dose. Irradiation with 1-MeV H^+ produced very few dislocation loops compared to the He, C, Al and Fe irradiations. Figure 10 shows the depth-dependent microstructure of alumina following irradiation with 1 MeV H^+ ions to a fluence of $1.7 \times 10^{22} \text{ H}^+/\text{m}^2$ at 650°C (0.03 dpa at $0.5 \mu\text{m}$ depth). Dislocation loops were not observed in the midrange regions of this specimen despite the presence of damage levels that were well above the threshold dose for observable defect cluster formation determined from irradiations with heavier ions (0.01 dpa). A low density of dislocation loops ($\sim 3 \times 10^{20}/\text{m}^3$) was observed at intermediate depths (~ 1 to $3 \mu\text{m}$) in another specimen irradiated with 1-MeV H^+ ions at an order of magnitude lower flux and fluence.²

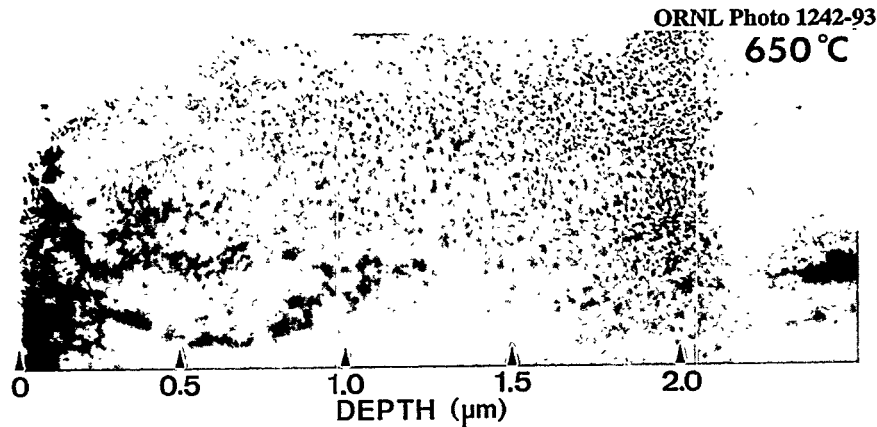


Fig. 9. Depth-dependent microstructure of Al_2O_3 irradiated with 3-MeV C^+ ions to a fluence of $3 \times 10^{19} \text{ C}^+/\text{m}^2$.

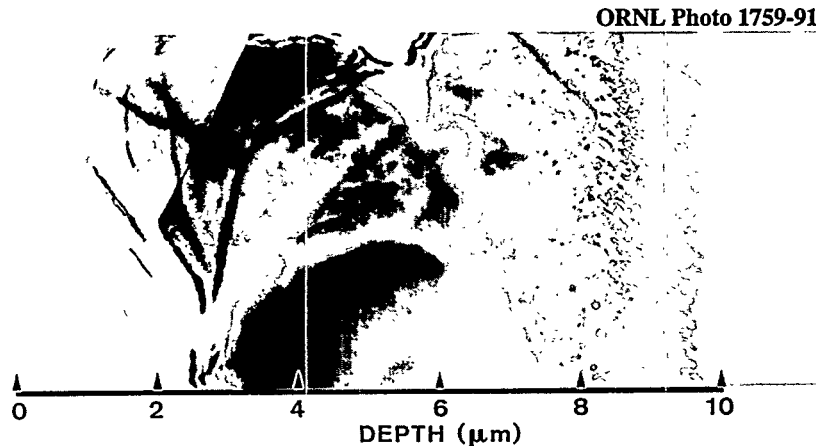


Fig. 10. Depth-dependent microstructure of Al_2O_3 irradiated with 1-MeV H^+ ions at 650°C to a fluence of $1.7 \times 10^{22} \text{ H}^+/\text{m}^2$. The particle flux was $\sim 6 \times 10^{17} \text{ H}^+/\text{m}^2\text{-s}$.

3.3 Investigation of the roles of ionizing vs. displacive radiation

The results on ion-irradiated spinel and alumina specimens indicate that the depth-dependent microstructural evolution in both materials is dependent on the mass and energy of the bombarding ion. This sensitivity to irradiation spectrum does not appear to be directly correlated with simple radiation parameters such as damage energy density, average primary knock-on atom recoil energy, displacement damage rate, or ionizing dose rate.² Another radiation parameter worth consideration is the electronic- to nuclear-stopping power ratio. As noted in Fig. 2, the ENSP ratio decreases with increasing ion mass and for a given ion is generally highest at the irradiated surface. Since the defect-free zones observed in spinel and alumina are more prominent for the lightest ions and are located adjacent to the irradiated surface, this suggests that the denuded zones may be associated with irradiation conditions which produce a high ENSP ratio.

Figure 11 summarizes the relation between the measured dislocation loop density and the calculated ENSP ratio in spinel and alumina specimens irradiated at 650°C. The data with arrows denote measurements where only upper limits could be estimated due to the extremely low loop densities ($<10^{18}/\text{m}^3$). Dislocation loop densities were measured at several different depths in each specimen in order to obtain data at several different ENSP ratios for a given ion (cf. Fig. 2). In the case of spinel, the dislocation loop density was observed to decrease rapidly for ENSP ratios greater than ~3 to 20. The loop density in alumina was observed to decrease rapidly for ENSP ratios greater than ~1000. The data for spinel suggest that the critical ENSP ratio for loop formation depends somewhat on the ion mass, with heavy ions exhibiting the lowest critical ENSP ratio.

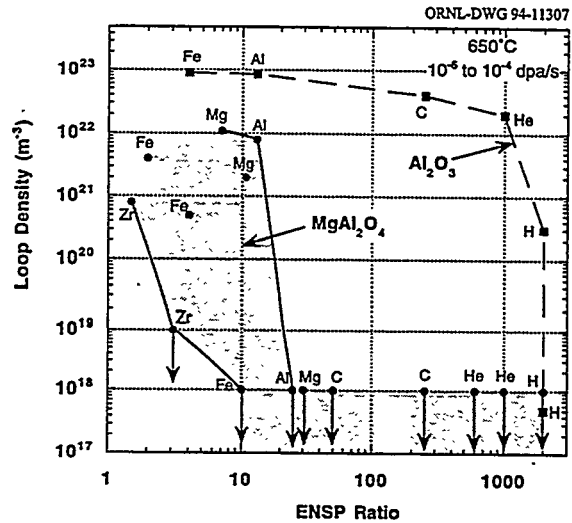


Fig. 11. Effect of electronic to nuclear stopping power on the dislocation loop density in MgAl_2O_4 and Al_2O_3 irradiated with single ion beams at 650°C.

The data summarized in Fig. 11 clearly indicate a strong irradiation-spectrum dependence for the microstructure of spinel and alumina. However, these single ion irradiation results cannot easily be extrapolated to fission and fusion reactor environments. In particular, the ionization produced in reactors has two distinct components, which are associated with the primary knock-on atoms (PKAs) and gamma rays, respectively. The PKAs produce intense, spatially localized ionization in the immediate vicinity of the PKA cascade, with most of the ionization in close proximity to the displaced atoms. On the other hand, gamma rays produce a rather uniform background of ionization throughout the material with little or no displacement damage. Table 2 compares the calculated ENSP ratios in a fusion reactor, fast fission reactor, and mixed spectrum (water cooled) fission reactor.²¹ The ENSP ratio in each facility was calculated both with and without the gamma ray ionization contribution.

The high flux of gamma rays present in a mixed-spectrum fission reactor has a significant impact on the total (macroscopically averaged) ENSP ratio. On the other hand, gamma rays have a much smaller effect on the calculated ENSP ratio in a fusion reactor due to the higher average PKA energy and the lower gamma ray flux compared to a mixed-spectrum fission reactor. Fast fission reactors exhibit behavior that is intermediate between the mixed-spectrum fission and fusion reactors

Table 2. Calculated ENSP ratio for alumina in the STARFIRE conceptual fusion reactor and the HFIR mixed spectrum and FFTF fast fission reactors²¹

<u>electronic to nuclear stopping power ratio</u>	<u>mixed spectrum reactor</u>	<u>fast reactor</u>	<u>fusion reactor (1st wall)</u>
total	100	4	13
PKA alone	4	2	11

Two scoping dual-ion beam irradiations were performed to experimentally investigate the importance of uniform versus localized ionization effects. Figure 12 compares the depth-dependent microstructure of spinel irradiated at 650°C with a single beam of 3.6-MeV Fe⁺ ions and dual beams of 1-MeV He⁺ and 3.6-MeV Fe⁺ ions. The Fe⁺ ion flux was 5x10¹⁵ Fe⁺/m²-s in both specimens. The He⁺/Fe⁺ particle flux ratio in the dual beam specimen was,¹⁷ which increased the calculated ENSP ratio at a depth of 0.5 μm from ~6 for the single Fe⁺ ion beam to 28 for the dual beams (Table 1). The calculated displacement damage from the He⁺ ion beam at a depth of 0.5 μm was only 4% of the displacements associated with the Fe⁺ ion beam. Both the single- and dual-beam specimen exhibited an identical defect-free zone adjacent to the irradiated surface that extended to a depth of ~0.4 μm. The density of the dislocation loops that were present in the midrange region (0.5 to 1 μm depth) of the two specimens was also similar. These results suggest that moderate levels of uniform ionization (macroscopically averaged ENSP ~28) have only a weak effect on the microstructural evolution in spinel when energetic displacement cascades (mean PKA energy ~10 keV) are produced.

The second scoping dual-ion irradiation used 1.8-MeV Cl⁺ and 1-MeV He⁺ ion beams, with a He⁺/Cl⁺ particle flux ratio of 105. This produced a calculated ENSP ratio of ~160 at a depth of 0.5 μm (Table 1). The calculated damage energy and ENSP ratio for 1.8-MeV Cl⁺ is similar to that for 3.6 MeV Fe⁺ at irradiation depths up to ~0.7 μm (Figs. 1 and 2), and the mean PKA energy for 1.8-MeV Cl⁺ ions in spinel (~8 keV) is also comparable to that for 3.6 MeV Fe⁺ ions. Figure 13 shows the depth-dependent microstructure of spinel irradiated with dual beams of Cl⁺ and He⁺ ions at room temperature and 650°C. The calculated damage level at a depth of 0.5 μm was 0.7 dpa in both specimens, with 78% of the displacements associated with the Cl⁺ ion beam. There were no observable defect clusters located within ~0.8 μm of the irradiated surface in the specimen irradiated at 650°C. According to the empirical relation established from the single ion irradiations (Fig. 11), the expected denuded zone width for spinel irradiated at 650°C with 1.8-MeV Cl⁺ ions alone would have been only ~0.4 μm. Therefore, intense uniform ionizing radiation (macroscopically averaged ENSP ~160) can apparently influence the microstructural evolution in spinel during elevated temperature irradiation. The room temperature dual beam irradiation produced a high density of small defect clusters that were uniformly distributed throughout the Cl⁺ ion irradiation region (Fig. 13), which suggests that these levels of uniform ionizing radiation (ENSP~160) do not have a significant impact on the microstructural evolution of spinel during room temperature irradiation.

4. Discussion

The data summarized in Fig. 11 clearly demonstrate that oxide ceramics such as Al₂O₃ and MgAl₂O₄ are sensitive to variations in the irradiation spectrum. This dependence on irradiation spectrum was observed in several specimens irradiated with different ion beams at the same calculated displacement damage rate or ionizing dose rate. Therefore, this phenomenon cannot be simply attributed to damage rate or ion beam heating effects. Perhaps the most significant implication of the observed irradiation spectrum dependence is that light ion (e.g. 1-MeV protons) and electron irradiations, which typically have ENSP ratios >1000, cannot be used to "simulate" the behavior of ceramics under fission or fusion neutron irradiation conditions, which have typical ENSP ratios of ~10. Recent electron and light ion irradiation studies performed on oxide ceramics that were irradiated with an applied electric field have found evidence for a permanent radiation-induced electrical degradation (RIED) in the electrical resistance after displacement damage levels of <0.01 dpa.^{1,23,24} Extrapolation of these high-ENSP results to fusion reactor conditions would not appear to be warranted, according to the microstructural observations summarized in Fig. 11.

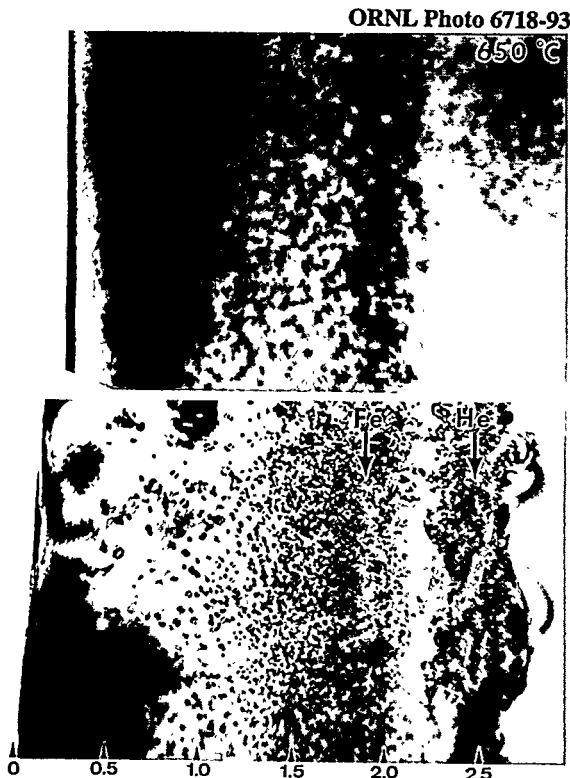


Fig. 12. Comparison of the depth-dependent microstructure of MgAl_2O_4 irradiated at 650°C with 3.6-MeV Fe^+ ions (top) and dual beams of 3.6-MeV Fe^+ and 1-MeV He^+ ions (bottom). The dual beam Fe^+/He^+ particle ratio was 17.

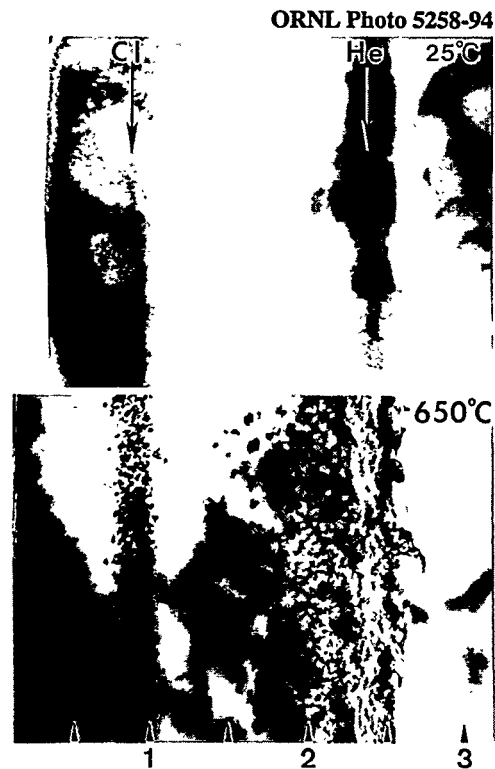


Fig. 13. Depth-dependent microstructure of MgAl_2O_4 irradiated at 650°C with dual beams of 1.8-MeV Cl^+ and 1-MeV He^+ ions at a He^+/Cl^+ particle ratio of 105.

It is important to demonstrate that the defect-free regions in the near surface regions of the ion-irradiated ceramics are not an artifact associated with localized ion beam heating effects, particularly since the defect-free zone width for a given ion has been observed to be related to the ion flux. If beam heating effects were significant, then the observed defect-free zone near the surface could be simply due to enhanced thermal diffusion which would promote point defect recombination and the evaporation of point defects from defect clusters. A simple one-dimensional heat transfer calculation shows that the temperature drop in spinel across a $1\ \mu\text{m}$ depth adjacent to the surface would be only $\sim 0.01^\circ\text{C}$ for the maximum beam heating conditions employed in the present experiments (30 MGy/s), assuming a thermal conductivity for irradiated spinel at 650°C of $K_{\text{th}}=5\ \text{W/m}\cdot\text{K}$. Furthermore, the specimen surface temperature during irradiation (monitored by the thermocouple on the stainless steel specimen) was always within 20°C of the heat-sinked substrate temperature for the target array. Additional evidence that the defect-free regions are not due to ion beam heating effects is obtained from observations that the defect-free zone widths for different ions could not be correlated with the beam heating.² For example, a high density of small dislocation loops was observed in the near-surface region of Al_2O_3 irradiated at 650°C with 2-MeV Al^+ ions at a beam power of 7 MGy/s (Fig. 8), whereas loops were not observed in alumina irradiated at 650°C with 1-MeV H^+ ions at a lower beam power of 3 MGy/s (Fig. 10).

The suppression of dislocation loop formation in oxide ceramics irradiated with light ions (high ENSP ratio) could in principle be due to two different effects; either a decrease in the defect production rate or an increase in the point defect recombination rate (e.g., due to ionization-enhanced diffusion). However, there is considerable evidence that the low loop density is not due to a low defect production rate. Optical spectroscopy measurements on Al_2O_3 indicate that the defect production rate (relative to the calculated displacement damage rate) of light ions such as protons is equal to or greater than that for heavier ions or neutrons.²⁵⁻²⁷ Buckley and Shaibani²⁸ noted that defect clusters did not form in spinel irradiated with

1 MeV electrons (ENSP ratio ~10,000), but preexisting dislocations climbed readily during the irradiation, indicating the presence of significant concentrations of point defects. Large defect clusters were observed in alumina irradiated with a low flux of protons after a dose of <0.01 dpa in the present study [2]. In addition, the few dislocation loops in spinel that were nucleated in regions with high ENSP ratios grew considerably during irradiation.^{2,14} These observations indicate that the suppressed dislocation loop density after light ion irradiation is not associated with a reduction in defect production but is instead due to difficulties in loop nucleation.

As mentioned in the introduction, several previous studies have reported that radiation effects in oxide ceramics are sensitive to the irradiation spectrum. The volumetric swelling in Al₂O₃ and MgO was found to be much lower in specimens irradiated at room temperature with light ions such as H⁺ than in specimens irradiated with heavier ions to the same calculated damage level.^{3,4} In addition, studies have shown that the volume expansion in Al₂O₃, BeO or MgO induced by heavy ion or fission neutron irradiation may be recovered by subsequent electron or H⁺ ion irradiation.^{3,4,29} Dislocation loops have not been observed in spinel following electron^{28,30,31} or proton^{2,20,32} irradiation (ENSP>1000) over a wide range of temperatures and damage levels. Electron irradiation has been shown to cause the disappearance of small dislocation loops produced in MgAl₂O₄ by Ar⁺ ion or neutron irradiation.^{7,31} In the present study, the effect of irradiation spectrum on the microstructural evolution in alumina and spinel was more pronounced at 650°C (~0.4 T_M) than at room temperature (~0.13 T_M). This sensitivity to irradiation temperature implies that the irradiation spectrum effect may be associated with point defect diffusion processes.

It is well established that the migration energy of a defect in semiconductors and insulators is strongly affected by the defect charge state.³³⁻³⁷ Similarly, it has been demonstrated that the diffusion coefficient (diffusivity) of hydrogen isotopes³⁸⁻⁴⁰ and vacancies⁴¹ in oxide insulators is greatly enhanced by ionizing radiation. Optical absorption measurements performed on oxide insulators have demonstrated that light ion irradiation spectra (high ionizing- to displacive-radiation ratio) preferentially produce a greater fraction of F⁺ centers, whereas heavy ions produce a larger proportion of F centers.^{4,6,42} In oxide insulators with predominantly ionic bonding, it is expected that the diffusivity of F centers (oxygen vacancy with two trapped electrons) should be significantly less than that of F⁺ centers (oxygen vacancy with one trapped electron).³⁴⁻³⁶ The precise physical mechanism responsible for ionization-enhanced diffusion in insulators is not known, although several different mechanisms have been proposed.³⁴ Regardless of the specific mechanism responsible for ionization-enhanced diffusion, the net result is that irradiation sources which produce large amounts of ionization compared to displacement damage are expected to be very effective in enhancing the point defect diffusion in oxide ceramic insulators. According to chemical rate theory calculations, a large increase in the diffusivity of point defects would enhance the amount of point defect recombination and thereby cause a dramatic reduction in the nucleation rate of defect clusters.

An additional possible mechanism for the observed suppression of defect cluster formation in spinel and alumina in highly ionizing irradiation environments may be an ionization-enhanced increase in the point defect recombination volume. Atomistic calculations of F and F⁺ centers in Al₂O₃ indicate that F⁺ centers exert a strong perturbation on surrounding lattice atoms.⁴⁴ It seems plausible that this lattice strain energy could lead to a higher rate of recombination of oxygen interstitials at F⁺ centers compared to F centers. The higher concentration of F⁺ centers in highly ionizing radiation environments [4,6,42] would therefore result in increased point defect recombination rates.

Further work is needed to identify the most appropriate parameter(s) for characterizing the irradiation spectrum. The electronic- to nuclear-stopping power appears to be a promising correlation parameter for single ion irradiation conditions (Fig. 11). This correlation suggests that dislocation loop formation is suppressed in spinel during irradiation at elevated temperatures (~650°C) at damage rates between 10⁻⁶ and 10⁻⁴ dpa/s if the ENSP ratio is greater than about 10. The corresponding critical ENSP ratio for alumina is about two orders of magnitude higher, i.e., 1000. However, dual beam irradiations (e.g. Figs. 12 and 13) have shown that this simple parameter does not accurately predict the microstructural behavior of oxide ceramics that are subjected to moderately intense uniform fields of ionizing radiation. The present results, taken together with recent results obtained by Fukumoto et al.,¹³ indicate that homogeneous ionizing radiation fields up to ENSP ratios of ~60 do not have a significant effect on the microstructural

evolution in spinel during irradiation at 600 to 650°C when most of the displacement damage is produced by energetic displacement cascades. As demonstrated in Fig. 13, homogeneous ionizing radiation fields apparently can influence the microstructural development in spinel during elevated temperature irradiation if the ionization field is very intense (ENSP~160).

As discussed elsewhere,² it is not surprising that the critical ENSP ratio derived from single ion irradiation experiments does not hold for dual beam irradiation experiments. In the single beam experiments, most of the ionization occurs along the bombarding ion path and is therefore in close proximity to the defects produced by displacement damage. On the other hand, the ionization in the dual beam experiments was more uniformly distributed throughout the specimen. Since most of the displacement damage in the dual beam irradiations was produced in spatially discrete collision cascades associated with the heavy ions, the localized ENSP ratio in the vicinity of the heavy ion collision cascades was less than the macroscopic ENSP ratio.

Additional radiation parameters which may be important in the suppression of dislocation loop formation are damage energy and irradiation flux. The nucleation of a stoichiometric dislocation loop in $MgAl_2O_4$ requires the presence of 7 interstitials.⁴⁵ Therefore, light ions (which produce diffuse radiation damage due to their low damage energy) might be expected to be less effective in producing dislocation loop nuclei compared to heavy ions (which produce relatively dense displacement cascades). Dalal et al.⁴² have concluded that the fraction of F^+ centers compared to F centers in alumina is enhanced as the defect generation rate is increased, due to a suppression of F center formation at high damage rates. According to the previous discussion, this would lead to enhanced defect mobilities (and point defect recombination) at high radiation fluxes. Irradiation flux effects have been observed in several cases in the present set of experiments. As noted in Section 3.1, the defect-free zone adjacent to the irradiated surface in Mg^{2+} -irradiated spinel was found to increase with increasing particle flux. Similarly, the dislocation loop density in proton-irradiated alumina was observed to decrease dramatically when the particle flux was increased by an order of magnitude (Section 3.2 and ref. [2]). Both of these experimental results imply that the point defect diffusivity (or point defect recombination rate) increased with increasing flux.

The present study shows that spinel becomes resistant to defect cluster formation at much lower ENSP ratios compared to alumina (Fig. 11). Previous ion and neutron irradiation studies have found that spinel is significantly more resistant than alumina to void swelling and dislocation loop formation.^{2,7,13,15,16,45} Since the ENSP ratio in all of these previous studies was equal to or greater than 4, this provides further confirmation of the empirical correlation between irradiated microstructure and ENSP ratio summarized in Fig. 11. The physical mechanism responsible for the higher sensitivity of spinel to ENSP ratio compared to ceramics such as MgO and Al_2O_3 is uncertain.² According to Kinoshita et al.,¹⁶ the most likely mechanisms are effective recombination of interstitials with the high concentration of structural vacancies present in spinel, and the large critical nucleus (7 interstitials) for the formation of a stable dislocation loop. Irradiation-assisted dissolution of small interstitial clusters in spinel has also been suggested to be playing a role.⁷ Additional possible mechanisms that would require further study include a high sensitivity to ionization-enhanced diffusion or a strong ionization-induced enhancement of the point defect recombination rate in spinel.

CONCLUSIONS

The microstructural changes in oxide ceramics induced by particle irradiation are dependent on the irradiation spectrum. Spinel is particularly resistant to defect cluster formation over a wide range of irradiation conditions. However, the present study clearly shows that high densities of dislocation loops can be produced in spinel in irradiation environments that produce relatively dense displacement cascades (with an associated low ratio of electronic- to nuclear-stopping power). Data obtained from single ion irradiations performed on spinel and alumina at 650°C at damage rates between 10^{-6} and 10^{-4} dpa/s have been correlated with the electronic- to nuclear-stopping power ratio. Dislocation loop formation is suppressed when the ENSP ratio exceeds ~10 and ~1000 for spinel and alumina, respectively. Due to the sensitivity of spinel and alumina to irradiation spectrum, data obtained on these materials during electron or light ion irradiation is most likely not representative of their behavior in a fission or fusion reactor environment.

Whereas alumina and spinel are sensitive to the localized irradiation spectrum associated with the primary knock-on atoms, they are not as strongly affected by homogeneous ionizing radiation. Moderate background levels of uniform ionizing radiation (averaged ENSP~30) do not significantly affect the microstructural evolution in spinel if most of the displacement damage is produced by energetic displacement cascades. However, high levels of uniform ionization (averaged ENSP~150) can modify the microstructural evolution in spinel, at least at elevated temperatures near 650°C. Since the irradiation spectrum in parts of a fusion reactor that are distant from the first wall are expected to have averaged ENSP ratios >100, this implies that uniform ionizing radiation effects may need to be considered when assessing the suitability of spinel for fusion energy applications.

The physical mechanism responsible for the sensitivity of alumina and spinel to irradiation spectrum is uncertain. The most likely explanation is that ionization enhanced diffusion (associated with high ENSP ratios) increases the amount of point defect recombination and thereby suppresses dislocation loop nucleation. Other possible mechanisms include damage energy effects (subcritical number of interstitials within a "cascade" region) and ionization-enhanced point defect recombination volumes.

ACKNOWLEDGEMENTS

The author thanks S. W. Cook for performing most of the ion irradiations, and A. T. Fisher, J. W. Jones, J. M. Cole and A. M. Williams for specimen preparation. This research was sponsored by the Office of Fusion Energy, U.S. Department of Energy, under contract DE-AC05-84OR21400 with Martin Marietta Energy Systems, Inc.

REFERENCES

1. S.J. Zinkle and E.R. Hodgson, *J. Nucl. Mater.* 191-194 (1992) 58.
2. S.J. Zinkle, *Nucl. Instr. Meth. Phys. Res. B* 91 (1994) 234.
3. G.W. Arnold, G.B. Krefft and C.B. Norris, *Appl. Phys. Lett.* 25 (1974) 540.
4. G.B. Krefft, *J. Vac. Sci. Technol.* 14 (1977) 533.
5. G.B. Krefft and E.P. EerNisse, *J. Appl. Phys.* 49 (1978) 2725.
6. R. Brenier, B. Canut, L. Gea, S.M.M. Ramos, P. Thevenard, J. Rankin, L. Romana and L.A. Boatner, *Nucl. Instr. Meth. Phys. Res. B* 80/81 (1993) 1210.
7. C. Kinoshita, *J. Nucl. Mater.* 191-194 (1992) 67.
8. M.B. Lewis, W.R. Allen, R.A. Buhl, N.H. Packan, S.W. Cook, and L.K. Mansur, *Nucl. Instr. Meth. Phys. Res. B* 43 (1989) 243.
9. J.F. Ziegler, J.P. Biersak and U.L. Littmark, *The Stopping and Range of Ions in Solids* (Pergamon Press, New York, 1985). The calculations in the present paper used the TRIM-90 version.
10. P. Agnew, *Phil. Mag.* A 65 (1992) 355.
11. M.J. Norgett, M.T. Robinson and I.M. Torrens, *Nucl. Eng. Design* 33 (1975) 50.
12. S.J. Zinkle, C.P. Haltom, L.C. Jenkins, and C.K.H. DuBose, *J. Electron Microsc. Techn.* 19 (1991) 452.
13. K. Fukumoto, C. Kinoshita, S. Maeda and K. Nakai, *Nucl. Instr. Meth. Phys. Res. B* 91 (1994) 252.
14. S.J. Zinkle, in *Fusion Reactor Materials Semiannual Prog. Report for period ending March 31, 1993*, DOE/ER-0313/14, p. 426.
15. H. Abe, C. Kinoshita and K. Nakai, *J. Nucl. Mater.* 179-181 (1991) 917.
16. C. Kinoshita, K. Fukumoto, K. Fukuda, F.A. Garner and G.W. Hollenberg, *Am. Cer. Soc. Symposium on Fabrication and Properties of Ceramics for Fusion Energy*, *J. Nucl. Mater.*, in press.
17. S.J. Zinkle, in *15th Int. Symp. on Effects of Radiation on Materials*, ASTM STP 1125, R.E. Stoller, et al., eds. (Amer. Soc. for Testing and Materials, Philadelphia, 1992) 749.
18. S.J. Zinkle, *J. Nucl. Mater.* 191-194 (1992) 645.
19. S.J. Zinkle, *J. Amer. Ceram. Soc.* 72 (1989) 1343.
20. S.J. Zinkle, in *Fusion Reactor Materials Semiannual Prog. Report for period ending March 31, 1991*, DOE/ER-0313/10, p. 302.
21. S.J. Zinkle and L.R. Greenwood, in *Fusion Reactor Materials Semiannual Prog. Report for period ending March 31, 1993*, DOE/ER-0313/14, p. 74.
23. E.R. Hodgson, *J. Nucl. Mater.* 179-181 (1991) 383.

24. L.W. Hobbs, F.W. Clinard, Jr., S.J. Zinkle and R.C. Ewing, *J. Nucl. Mater.* 216 (1994) 291.
25. D.W. Muir and J.M. Bunch, in *Radiation Effects and Tritium Technology for Fusion Reactors*, CONF-750989, Vol. II, eds. J.S. Watson and F.W. Wiffen (Nat. Tech. Inf. Serv., Springfield, VA, 1976) p. 517.
26. T.F. Luera, *J. Appl. Phys.* 51 (1980) 5792.
27. P. Agnew, *Nucl. Instr. Meth. Phys. Res. B* 65 (1992) 305.
28. S.N. Buckley and S.J. Shaibani, *Philos. Mag. Lett.* 55 (1987) 15.
29. D.G. Walker, *J. Nucl. Mater.* 14 (1964) 195.
30. S.J. Shaibani, D. Phil. Thesis, Univ. Oxford, UK (1986).
31. Y. Satoh, C. Kinoshita and K. Nakai, *J. Nucl. Mater.* 179-181 (1991) 399.
32. P.A. Knight, D. Phil. Thesis, Univ. Oxford, UK (1989).
33. J.W. Corbett and J.C. Bourgoin, *IEEE Trans. Nucl. Sci. NS-18*, No. 6 (1971) 11.
34. J.W. Corbett and J.C. Bourgoin, *Rad. Effects* 36 (1978) 157.
35. J.M. Vail, R.J. Brown and C.K. Ong, *J. de Phys.* 34 (1973) C9-83.
36. N. Itoh, in *Dynamic Effects of Irradiation in Ceramics*, Los Alamos National Lab. Report LA-UR-92-4400 (1992) p. 3.
37. L. Gea, C.R.A. Catlow, S.M.M. Ramos, B. Canut and P. Thevenard, *Nucl. Instr. Meth. Phys. Res. B* 65 (1992) 282.
38. Y. Chen, M.M. Abraham and H.T. Tohver, *Phys. Rev. Lett.* 37 (1976) 1757.
39. Y. Chen, R. Gonzalez and K.L. Tsang, *Phys. Rev. Lett.* 53 (1984) 1077.
40. Y. Chen and R. Gonzalez, *Intern. Mat. Res. Soc. Symp. on Frontiers of Materials Science*, Tokyo, 1993, in press.
41. S. Clement and E.R. Hodgson, *Phys. Rev. B* 36 (1987) 3359.
42. M.L. Dalal, M. Rahmani and P.D. Townsend, *Nucl. Instr. Meth. Phys. Res. B* 32 (1988) 61.
43. R.E. Stoller and G.R. Odette, *J. Nucl. Mater.* 141-143 (1986) 647.
44. E.A. Kotomin, A.I. Popov and A. Stashans, *J. Phys. Condensed Mat.*, in press.
45. L.W. Hobbs and F.W. Clinard, Jr., *J. de Phys.* 41 (1980) C6-232.